- 1 "Influence of the NO/NO₂ Ratio on Oxidation Product Distributions under High-NO Conditions"
- 3 Kevin J. Nihill, 1* Qing Ye, 1 Francesca Majluf, 2 Jordan E. Krechmer, 2 Manjula R. Canagaratna, 2
- 4 Jesse H. Kroll¹

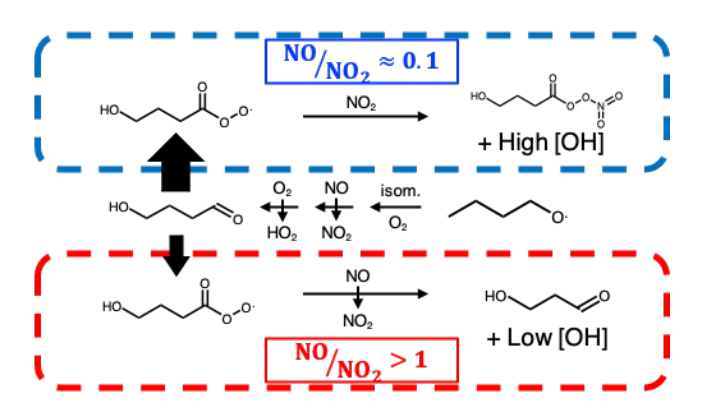
2

5

9

11

- 6 1. Department of Civil and Environmental Engineering, Massachusetts Institute of Technology,
- 7 77 Massachusetts Avenue, Cambridge, MA, USA
- 8 2. Aerodyne Research, Inc., 45 Manning Rd., Billerica, MA, USA
- 10 *Email address for corresponding author: kevin.j.nihill@gmail.com
- 12 Synopsis: Simple, well-constrained organic oxidation systems are probed to measure the
- influence of the NO/NO₂ ratio on product distributions.
- 14 <u>Keywords:</u> oxidation; NO_x; peroxy radicals; alkyl nitrites; secondary organic aerosol
- 15 <u>Table of Contents Figure:</u>



16

Abstract

17

18

19

20

21

22

23

24

25

26

27

28

29

30

31

32

33

34

35

Organic oxidation reactions in the atmosphere can be challenging to parse due to the large number of branching points within each molecule's reaction mechanism. This complexity can complicate the attribution of observed effects to a particular chemical pathway. In this study, we simplify the chemistry of atmospherically relevant systems by generating individual alkoxy radicals via alkyl nitrite photolysis (in order to limit the number of accessible reaction pathways) and measuring their product distributions under different NO/NO₂ ratios. Known concentrations of NO in the classically "high NO" range are maintained in the chamber, thereby constraining first-generation RO₂ (peroxy radicals) to react nearly exclusively with NO. Products are measured in both the gas phase (with a Proton-Transfer Reaction Mass Spectrometer) and the particle phase (with an Aerosol Mass Spectrometer). We observe substantial differences in measured products under varying NO/NO₂ ratios (from ~0.1 to >1); along with modeling simulations using the Master Chemical Mechanism (MCM), these results suggest indirect effects of NO_x chemistry beyond the commonly-cited RO₂ + NO reaction. Specifically, lower NO/NO₂ ratios foster higher concentrations of secondary OH, higher concentrations of peroxyacyl nitrates (PAN, an atmospheric reservoir species), and a more highly oxidized product distribution that results in more secondary organic aerosol (SOA). The impact of NO_x concentration beyond simple RO₂ branching must be considered when planning laboratory oxidation experiments and applying their results to atmospheric conditions.

Introduction

Atmospheric organic oxidation mechanisms are highly complex, involving numerous reaction branching points and multiple generations of oxidation for an individual compound.^{1,2} The large number of products formed from a given compound, which are a strong function of the compound's structure and of reaction conditions, poses substantial challenges for the elucidation of detailed mechanisms and the prediction of key secondary species such as ozone and secondary organic aerosol (SOA).^{3–5}

A key branch point in atmospheric oxidation mechanisms involves organic peroxy (RO₂) radicals, which can react bimolecularly with NO_x, HO₂, or other RO₂, or undergo unimolecular reactions. ^{5,6} The role of NO_x in RO₂ fate is of particular interest as NO_x is present across a wide range of concentrations in the atmosphere, varying from ppt levels in remote regions ⁷ to tens or even hundreds of ppb in urban settings and in biomass burning plumes. ⁸⁻¹¹ Under high NO concentrations (i.e., NO mixing ratios in the ppb level or higher), the dominant reaction pathway for peroxy radicals is RO₂ + NO \rightarrow RO + NO₂, ^{4,5,12-15} with a minor contribution from the reaction RO₂ + NO \rightarrow RONO₂. ¹⁶⁻¹⁸ Recent work on NO_x has gone beyond absolute NO_x levels in order to focus on the role of the NO/NO₂ ratio in reaction mixtures. While some studies have explored the role of this ratio in terms of important subsets of atmospheric mechanisms (e.g., SOA, highly oxidized molecules), ¹⁹⁻²¹ the NO/NO₂ ratio has not been investigated in terms of its effects on the overall product distribution. This limits our ability to accurately predict how reaction systems respond to changes in NO_x levels, and risks leading to inaccurate recreations of "polluted conditions" in laboratory studies.

Here, we seek to better understand the detailed role of NO_x , and specifically the NO/NO_2 ratio, in influencing product distributions; this requires a reaction scheme in which the initiating

chemistry is independent of NO_x and the product distribution has a manageable complexity. We accomplish this via the photolysis of alkyl nitrite (RONO) compounds^{22,23} to directly generate alkoxy radicals (key intermediates in organic oxidation) in the presence of known concentrations of NO. For larger RO radicals, such as the *n*-butoxy radical shown in Figure 1, the dominant channel is isomerization to form an RO_2 radical, which can subsequently undergo a number of reactions. This method involves no direct introduction of gas-phase oxidants, and the generation of a single initial organic radical (as opposed to a mixture of radicals arising from multiple potential OH-reaction sites, which is typical for oxidant-initiated chemistry), greatly simplifying the product distribution compared to traditional laboratory oxidation studies.^{22–24} Moreover, it enables control over the NO_x levels in a manner that does not affect the initial reaction rate, thus facilitating the role of NO_x to be studied directly.

These experiments are run under two NO concentrations, both within the classical "high NO" limit ([NO] \gg 1 ppb), but representing NO/NO₂ ratios that differ by over an order of magnitude. Such high concentrations of NO ensure that the initially-formed RO₂ to react almost exclusively with NO, thus making it possible to probe these simple RO₂ systems as a function of changing NO/NO₂ ratio. Such systems can provide insight into the mechanisms underlying the NO_x-dependence of VOC oxidation chemistry, specifically elucidating the role of the NO/NO₂ ratio in environmental chamber studies; this in turn may help to foster more realistic NO_x conditions in chamber studies simulating the formation of SOA and other products under high-NO_x reaction conditions.

$$\begin{array}{c} \text{Alkyl nitrite} \\ \text{Alkoxy radical} \\ \text{C}_{4}\text{H}_{9}\text{O}_{2} \\ \text{Alkoxy radical} \\ \text{C}_{4}\text{H}_{9}\text{O}_{2} \\ \text{O}_{4}\text{H}_{9}\text{O}_{3} \\ \text{O}_{5}\text{O}_{4}\text{H}_{9}\text{O}_{3} \\ \text{O}_{6}\text{O}_{6}\text{O}_{6}\text{O}_{6}\text{O}_{6} \\ \text{O}_{6}\text{O}_{6}\text{O}_{7}\text{O}_{7} \\ \text{O}_{7}\text{O}_{7}\text{O}_{7}\text{O}_{7}\text{O}_{7}\text{O}_{7} \\ \text{O}_{7}\text{O}_{7}\text{O}_{7}\text{O}_{7}\text{O}_{7} \\ \text{O}_{7}\text{O}_{7}\text{O}_{7}\text{O}_{7} \\ \text{O}_{7}\text{O}_{7}\text{O}_{7}\text{O}_{7} \\ \text{O}_{7}\text{O}_{7}\text{O}_{7}\text{O}_{7}\text{O}_{7} \\ \text{O}_{7}\text{O}_{7}\text{O}_{7}\text{O}_{7} \\ \text{O}_{7}\text{O}_{7}\text{O}_{7}\text{O}_{7}\text{O}_{7} \\ \text{O}_{7}\text{O}_{7}\text{O}_{7}\text{O}_{7}\text{O}_{7}\text{O}_{7} \\ \text{O}_{7}\text{O}_{7}\text{O}_{7}\text{O}_{7}\text{O}_{7} \\ \text{O}_{7}\text{O}_{7}\text{O}_{7}\text{O}_{7}\text{O}_{7} \\ \text{O}_{7}\text{O}_{7}\text{O}_{7}\text{O}_{7}\text{O}_{7} \\ \text{O}_{7}\text{O}_{7}\text{O}_{7}\text{O}_{7}\text{O}_{7}\text{O}_{7} \\ \text{O}_{7}\text{O}_{7}\text{O}_{7}\text{O}_{7}\text{O}_{7} \\ \text{O}_{7}$$

Figure 1. Major first-generation products of the photolysis of *n*-butyl nitrite. The resulting alkoxy radical will primarily isomerize, yielding an RO₂ radical that can undergo a number of different reactions. Red arrows indicate dominant reaction pathways under the high-NO conditions employed herein.

Materials & Methods

Chamber Conditions

Reactions were carried out in a 150 L PFA chamber (described in detail elsewhere²⁵) surrounded by an array of twelve 340 nm UV lights (Q-lab). The spectral distribution of these lamps overlaps well with the absorption spectrum of precursor RONO compounds,²⁶ ensuring rapid photolysis. UV irradiation in this wavelength range (290-400 nm) involves relatively lowenergy photons, limiting the extent of vibrationally/electronically excited products.^{22,26}

Experiments were run at room temperature (~25 °C) and pressure (~1 atm) in semi-batch mode, with sampling flows balanced by an equal input of pure, low-RH (< 1%) air, resulting in a chamber residence time of approximately 15 minutes. Prior to each experiment, the chamber was

flushed with pure, dry air for at least one hour. Additionally, the internal walls of the chamber were cleaned between groups of experiments by flooding with O₃ and H₂O while irradiating overnight.

Experiments were run under one of two NO concentrations to ensure the dominance of the RO₂ + NO reaction. In "higher-NO" experiments (NO/NO₂ > 1), the chamber was maintained at a constant concentration of ~1 ppm NO by continual addition of NO prior to and throughout the run. In "lower-NO" experiments (NO/NO₂ \approx 0.1, roughly representative of NO/NO₂ ratios in ambient conditions²⁷), the only source of NO was from the photolysis of the RONO precursor, resulting in a steady state concentration of ~40 ppb with the lights on. (Full NO/NO₂ ratios throughout a typical experiment are provided in the SI.) At these classically "high NO" conditions, reactions with HO₂ and isomerization reactions cannot compete with the RO₂ + NO pathway.^{28–30} In addition to restricting accessible RO₂ reaction pathways, these high NO concentrations further limit reaction complexity by shortening the lifetime of secondary oxidants O₃ and NO₃, which could otherwise contribute to oxidation and SOA formation.³¹ However, as described below, there is still sufficient secondary OH formation in the reaction mixture to affect the product distributions.

Prior to injection of RONO, the chamber was filled with dry ammonium sulfate seed particles to provide surface area to promote condensation of low-volatility products, and to allow for correction for particle losses due to dilution and wall loss. Polydisperse (NH₄)₂SO₄ seed was added to the system by atomizing 1 g/L aqueous solution with a constant output atomizer (TSI) and passing the output through a desiccant prior to entering the chamber. Following this, ~400 ppb of the RONO compound (described below) was injected into a septum and carried by a stream of air into the chamber where it was allowed to mix in the dark for two minutes. Finally, the lights

were turned on to initiate the reaction and remained on for the duration of the experiment (approximately one hour).

Instrumentation

Product distributions were measured by a suite of real-time mass spectrometric instruments. Particle mass and composition was measured by an Aerodyne high-resolution Aerosol Mass Spectrometer (AMS),³² run in "V mode" (mass resolving power of ~3000). Known ion fragmentation of various ions detected by the AMS enabled extraction of the elemental ratios H/C and O/C,³³ thereby allowing the ensemble oxidation state of the SOA to be measured throughout the course of the reaction.³⁴ AMS organic signal was normalized to sulfate concentration in order to account for chamber dilution, wall loss, and changes in the AMS collection efficiency.

Products in the gas phase were measured by a Vocus Proton-Transfer Reaction High Resolution Time-of-Flight Mass Spectrometer (PTR-MS),³⁵ which is capable of providing speciated measurements of individual molecules and is exceptionally sensitive to volatile compounds with relatively low carbon oxidation states.³⁶ In order to maximize its sensitivity to low-volatility compounds, the Vocus inlet is heated to 100 °C to reduce wall losses due to gas-wall partitioning. (The loss of gas-phase species to chamber walls and instrument inlets is expected to be minor in these experiments, as described in the SI.) The pure RONO precursor is itself only weakly detected by the Vocus as a protonated molecule ([M+H]⁺); it is instead primarily detected as a combination of an aldehyde (via loss of -NO, [M - NO]⁺) and an alkene (via loss of -ONO, [M - ONO]⁺), as observed in previous work.³⁷ One challenge is that the aldehyde species is also a product formed from the oxidation of the alkoxy radical. In order to deconvolute the contributions to this ion from the RONO precursor and aldehyde product, the aldehyde time series was fit with

a function that included a decay factor for the precursor and a growth factor for the product, as shown in Figure S4.

The Vocus was calibrated by equating the total precursor signal (counts per second) prior to photolysis to the known amount of precursor injected into the chamber (~400 ppb); this ratio was then directly applied to all product compounds as an approximate calibration factor. Given the relatively limited range of oxidized functionalities and the tendency of PTR calibration factors to vary only up to a factor of ~2 in either direction,³⁸ the use of a single calibration factor for all species is assumed to be a reasonable approximation. While this approach introduces some error into the quantification of individual product species, differences in measured levels of a given compound in both the higher- and lower-NO experiments are independent of calibration, thus allowing for a direct comparison between experiments run under different NO/NO₂ ratios.

In addition to the mass spectrometric measurements of the organic species, concentrations of NO and NO₂ were measured with one of two NO_x monitors (Thermo Fisher Scientific, Model 42*i* for measuring NO and NO_x, or 2B Technologies Model 405 nm for measuring NO and NO₂; see SI, section 2 for more details). The presence of NO_y in the chamber interfered with precise NO₂ measurements (details regarding the deconvolution of interfering RONO signal from the pure NO_x signal can be found in the SI, section 2); however, an order-of-magnitude difference in NO/NO₂ ratios between the two sets of experiments was still clearly observed. All gas-phase data collected by the NO_x monitor and Vocus-PTR were corrected for dilution (with the exception of NO in the higher-NO experiments, in which it is part of the dilution flow) using an experiment-specific dilution rate based on chamber volume and input flow-rates.

Alkyl Nitrite Precursors

Experiments were carried out with four straight-chain alkyl nitrites (n-butyl, n-pentyl, n-hexyl, and n-decyl nitrite). This study focuses on n-butyl nitrite as a simple model for gas-phase systems; n-pentyl nitrite was employed in order to examine trends across another gas-phase system, whereas the larger nitrites (n-hexyl and n-decyl nitrite) were studied to examine SOA formation. 23,39,40

N-butyl nitrite and *n*-pentyl nitrite were purchased directly (Sigma-Aldrich) and used without further purification; *n*-hexyl nitrite and *n*-decyl nitrite were not commercially available, and so were synthesized in the laboratory. Synthesis of alkyl nitrites was carried out by Onitrosation of the parent alcohol species (Sigma-Aldrich), as described elsewhere. Confirmation of the conversion of alcohol to alkyl nitrite was made by UV-Vis spectroscopy of the RONO mixture, with spectra similar to those reported by Heicklen. After synthesis, RONO species were wrapped in foil to limit exposure to ambient light and stored in the refrigerator until they were used in an experiment, which typically occurred within 3 hours of synthesis to maintain integrity.

Master Chemical Mechanism Simulations

Simulations using the Master Chemical Mechanism (MCM v3.2)^{43,44} run using the F0AM package⁴⁵ in MATLAB were employed in order to map out the reaction mechanisms for individual NO regimes and precursors. These simulations were exploited to further probe differences between lower- and higher-NO conditions, and for estimating species that are not detectable by our instruments (e.g., OH).

Because the precursor RONO species used in these experiments are not included in the MCM, the experimentally-determined photolysis rate of the RONO (as measured by the Vocus)

was used to introduce RO and NO into the simulation at a controlled rate; in higher-NO experiments, the concentration of NO in the simulation was fixed at 1 ppm. Simulations included a dilution factor in order to recreate chamber conditions.

Results & Discussion

Average NO/NO₂ ratios are determined by comparisons of NO_x monitor measurements and MCM simulations. For lower-NO experiments, the NO/NO₂ ratio quickly reaches a steady-state value of \sim 0.1 with the lights turned on; for higher-NO experiments, the constant flow of 1 ppm NO into the chamber results in NO/NO₂ > 1 throughout the experiment (Table S1 and Figures S2-3).

Figure 2 shows the major gas-phase products (weighted by ppb carbon) from the photolysis of *n*-butyl nitrite, under lower-NO (panel a) and higher-NO (panel b) conditions. These major ions account for ~60% (lower-NO) and ~75% (higher-NO) of measured secondary carbon; stacked plots of all detected product traces are provided in Figure S5. In both experiments, the precursor reacts away at a roughly equivalent rate (average decay constant $\sim 2 \times 10^{-3} \text{ s}^{-1}$), which is also the case for all other precursors in these experiments; this decay is consistent with precursor loss by photolysis that exhibits no dependence on NO. While the precursor RONO is capable of reacting directly with OH generated in the reaction mixture, the concentrations of OH (predicted by MCM simulations and shown in Figure S6) and small rate constant ($k_{\text{RONO+OH}} < 3 \times 10^{-12} \text{ cm}^3 \text{ molec}^{-1} \text{ s}^{-1}$)⁴⁶ suggest that this pathway is minor, accounting for only 5-10% of RONO loss.

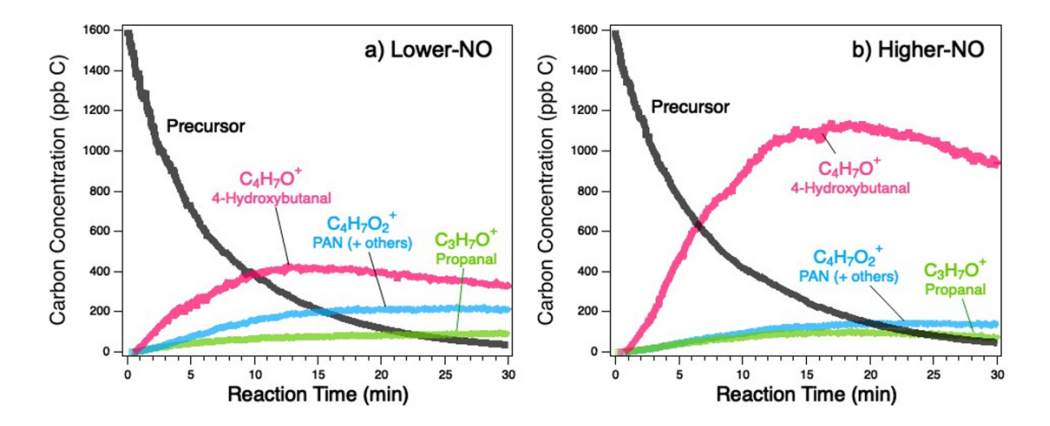


Figure 2. Carbon-weighted concentrations of the precursor and major product ions from the photolysis of *n*-butyl nitrite under (a) lower-NO and (b) higher-NO conditions, as measured by Vocus-PTR. Traces are labeled with the ion detected by the Vocus and the corresponding chemical identity; see SI for a detailed discussion of molecular assignments for Vocus ions.

The RO radicals formed from RONO photolysis are expected to undergo the same reactions in both the lower-NO and higher-NO experiments (Figure 1). A fraction (\sim 20%) of the RO radicals are expected to react directly with O₂ to form butanal, but because the detected ion is the same as one of the ions from the precursor (as discussed above), the exact contribution of this minor channel is not well-constrained in these experiments. The majority of the RO radicals will isomerize, forming a hydroxy-substituted RO₂ radical. The high concentration of NO in both cases ensures that this RO₂ will react with NO, predominantly forming 4-hydroxybutanal (C₄H₈O₂, primarily detected as the dehydrated C₄H₇O⁺ ion by the Vocus⁴⁷). A fraction of the RO₂ will react with NO to form the 4-hydroxynitrate product (C₄H₉NO₄), but the yield is expected to be very small (\sim 1%),⁵ and such oxygenated nitrates are poorly detected by the Vocus.³⁶ The other RO₂ channels are not expected to be competitive: under both lower- and higher-NO conditions, the RO₂ + HO₂ and RO₂ isomerization channels are expected to contribute negligibly (<<1%) to the

reaction, and the peroxynitrate formed from $RO_2 + NO_2$ is too short-lived to contribute to the reaction mixture.^{5,20}

Despite the identical chemistry of the initially-formed RO and RO₂ radicals under the two NO regimes, there are substantial differences in their product distributions (Figure 2). (These differences are much larger than expected run-to-run variability, as duplicate runs show very little variation, as shown in Figure S7.) Most notably, while the major product in both cases is 4-hydroxybutanal (C₄H₇O⁺), it is present in much greater concentrations under higher-NO conditions. This disparity arises from differences not in formation yield but in loss rates; as shown in Figure S8, the initial formation rate of this compound is the same in the two cases, as expected from the RO₂ chemistry (Figure 1). Because the main chemical sink of hydroxybutanal is oxidation by OH (photolysis is only a very minor channel, estimated to be ~2% by MCM), the more rapid loss of this species under lower-NO conditions implies that lower-NO experiments involve higher concentrations of OH.

While the reaction system used here did not involve the initial generation of OH, secondary OH can be formed from the reaction of HO₂ (formed after the isomerization of the hydroxyalkoxy radical, Figure 1) with NO. MCM simulations predict that, under higher-NO conditions, OH is produced at a greater rate (by a factor of ~2.5), but that the OH reactivity is higher still (largely due to increased NO_x levels), leading to lower levels of OH overall (Figure S6). The prediction of higher OH levels under lower-NO conditions is further confirmed by the higher mean carbon oxidation state $(\overline{OS}_C)^{34}$ of the measured product distribution under lower-NO conditions; this trend of increased oxidation under lower NO/NO₂ ratios is also observed for the photolysis of *n*-pentyl nitrite (Figure S9). While this experimental system is not a major source of secondary OH in the

atmosphere, these differences indicate the role of the NO/NO_2 ratio in governing product distributions beyond the initial $RO_2 + NO$ reaction.

248

249

250

251

252

253

254

255

256

257

258

259

260

261

262

263

264

265

266

267

268

269

The photolysis of *n*-butyl nitrite produces no observable SOA, consistent with the small carbon skeleton and consequently high volatility of the products formed. Larger nitrites ($n_C > 5$), however, can form products with sufficiently low volatilities to contribute to the formation of SOA. 23,40 This is evident from Figure 3, which shows SOA formation from the photolysis of npentyl nitrite, n-hexyl nitrite, and n-decyl nitrite under lower- and higher-NO conditions. As in the gas-phase, the particle-phase measurements exhibit differences under the two NO regimes. All three precursors exhibit higher SOA production under lower-NO conditions as measured in the plateau region (i.e., after 10 minutes). Most notably, n-pentyl nitrite produces no measurable SOA under higher-NO conditions but measurable levels under lower-NO conditions. Additionally, nhexyl nitrite and n-decyl nitrite produce approximately 64% and 78% more SOA under lower-NO conditions, respectively. (As shown in the SI, the observed differences are greater than the uncertainty in the measurements.) As with results in the gas phase, this can be attributed to higher levels of secondary OH under lower-NO conditions, leading to more highly oxidized products that partition into the particle phase. This observation is also in agreement with previous studies that see SOA yields for most systems as being inversely correlated with NO concentrations. 12,19 Further, the mean oxidation state of measured SOA formed from n-decyl nitrite (the only precursor for which SOA formation is large enough for a precise measurement of $\overline{OS_C}$) is greater under lower-NO conditions (-1.34) than under higher-NO conditions (-1.45); this is consistent with the observed average oxidation states in the gas phase product distributions.

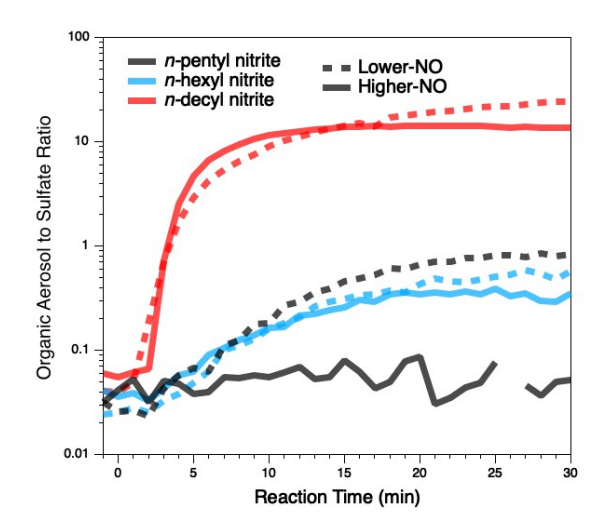


Figure 3. AMS total organic time series under lower-NO (dashed lines) and higher-NO (solid lines) concentrations. Traces are normalized to sulfate concentration to account for wall losses, collection efficiency, and dilution. *N*-butyl nitrite produces no organic aerosol, similar to *n*-pentyl nitrite under higher-NO conditions, and so it is not shown.

The differences between the oxidation product distributions demonstrate the influence of NO_x chemistry beyond the dominance of NO pathways for the initial RO_2 reaction; such differences are seen in both the gas phase and in the particle phase. To further investigate the influence of NO_x on VOC oxidation product distributions, Figure 4a compares the average (carbon-weighted) concentrations of different gas-phase products from n-butyl nitrite photolysis under the two different NO levels. The higher-NO regime is characterized by a dominant concentration of 4-hydroxybutanal ($C_4H_7O^+$) due to lower levels of OH and therefore a longer lifetime, as discussed above (Figure 2 and S8). Conversely, greater OH concentrations under lower-NO condition result in a wider variety of products and greater concentrations of products with higher oxidation states (Figures 4 and S10), providing the basis for the larger \overline{OS}_C (Figure S9). This includes multigenerational oxidation products such as propanal ($C_3H_7O^+$, formed from

the reaction of butanal + OH), which has a greater concentration under lower-NO conditions (Figures 2, 4).

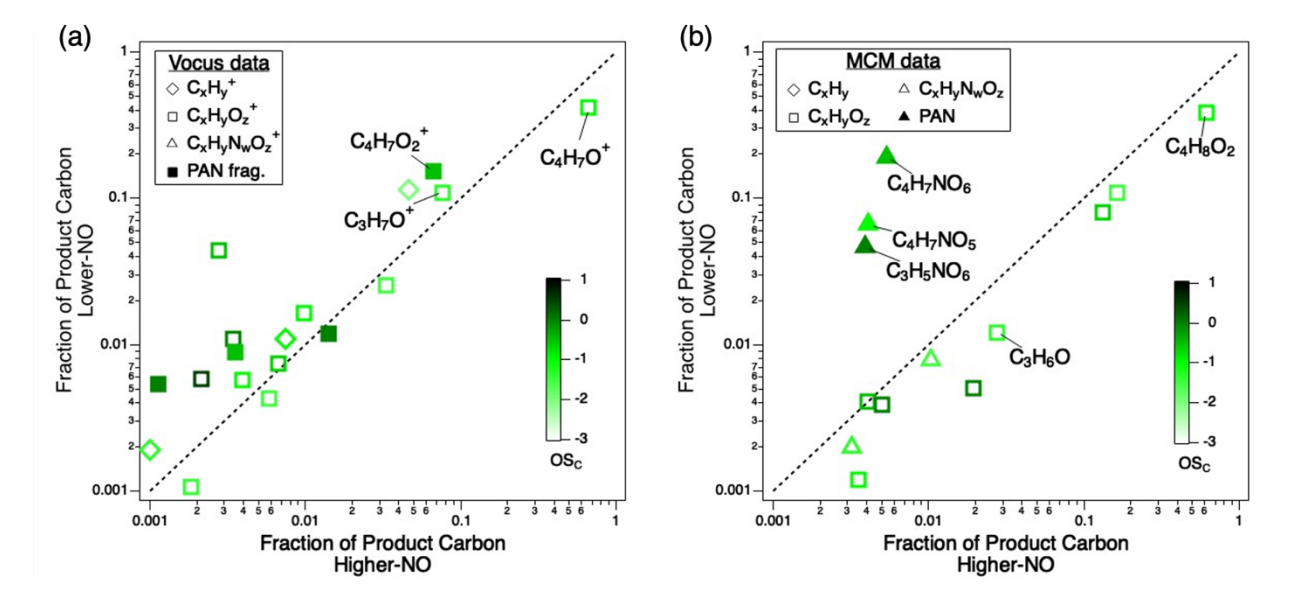


Figure 4. Correlation plots for fractions of gas-phase products under lower-NO vs. higher-NO regimes, averaged over the entire experiment. Panel (a): Vocus-PTR observations. Panel (b): MCM predictions. Markers are shaped according to class of molecule and are colored by average carbon oxidation state $(\overline{OS_C})$. Labeled compounds in panel (a) are the same as those in Figure 2; all other compounds are discussed in detail in the SI. MCM results (panel b) include labels for PAN species (solid triangles); potential PAN fragments are represented by filled markers in panel (a). Dashed line represents the 1:1 ratio.

Figure 4b shows the same comparison of product distributions in the two NO regimes, but based on MCM predictions rather than experimental data. While detailed comparisons between Vocus and MCM distributions are beyond the scope of this work, the fact that the MCM predicts fewer major products than are measured by the Vocus is likely attributable to individual molecules

being detected as multiple fragment ions by the Vocus, and to the generally simplified chemistry of the MCM. Overall consistencies between the MCM simulations and Vocus data include a predominance of 4-hydroxybutanal ($C_4H_8O_2$) occurring under both NO regimes, with a greater concentration of this species under higher-NO conditions. These general results are similar to those from the *n*-pentyl nitrite system (Figures S11-12).

The most pronounced differences between the two NO_x regimes in Figure 4b are the PAN compounds (e.g., C₄H₇NO₆), which are considerably more prevalent under lower-NO conditions and, as discussed below, are second-generation oxidation products. PANs are not detected directly by PTR-MS, but can be detected by known fragmentation patterns.^{48–50} One example is C₄H₇O₂+, a predicted tracer ion for C₄H₇NO₆ (analogous to C₂H₃O⁺ serving as a tracer ion for peroxyacetyl nitrate, C₂H₃NO₅);⁴⁸ its identity as a PAN is further suggested by the induction period observed in its time series (Figure 2), which is indicative of later-generation products. Potential PAN fragments are represented by shaded squares in Figure 4a. (A more detailed discussion of these other PAN-related ions detected by the Vocus can be found in the SL) Although these compounds are more prevalent under lower-NO conditions, the measured differences are not as dramatic as predicted by MCM simulations. This may be because these ions are not unique to PAN fragments, as they may be formed from the fragmentation of other product ions (e.g., acyl compounds), potentially resulting in a shift towards the 1:1 line. For example, while C₄H₇O₂+ is a tracer for C₄H₇NO₆, it could be a tracer for 4-hydroxybutanoic acid and similar species as well.

PAN formation, from the reaction of acylperoxy radicals with NO₂, is not shown in Figure 1, since acylperoxy radicals are not formed as first-generation radicals from alkoxy radical isomerization. Instead, acylperoxy radicals will be formed from the oxidation of first-generation aldehyde species, such as 4-hydroxybutanal:

 $C_4H_8O_2$ (hydroxybutanal) + OH + $O_2 \rightarrow C_4H_7O_4$ (acylperoxy radical) (1)

327 $C_4H_7O_4$ (acylperoxy radical) + $NO_2 \rightleftharpoons C_4H_7NO_6$ (PAN) (2)

Rates of PAN formation are observed (Figure 4a) and predicted (Figure 4b) to be substantially greater under lower-NO conditions. This is a result of two factors: The difference in OH levels (as discussed above), which controls the formation of acylperoxy radicals, and the subsequent chemistry of the acylperoxy radical. When NO_x is present, acylperoxy radicals are limited to two reactions: reaction with NO₂ to form PAN, and reaction with NO to form acyloxy radicals. The concentrations of PAN species are thus a strong function of the NO/NO2 ratio, as discussed elsewhere. 4,14,19,20 Under higher-NO conditions, this ratio is sufficiently high (NO/NO₂ > 1) that the acylperoxy + NO pathway is dominant, limiting the formation of PAN. Under lower-NO conditions (NO/NO₂ \approx 0.1), there is considerable competition from the acylperoxy + NO₂ pathway, resulting in the accumulation of PAN species. Thus, PAN formation is more favored under lower-NO than under higher-NO conditions because it fosters higher OH levels and a greater rate of the acylperoxy + NO₂ reaction. This additional PAN formation, which is observed in the measurements and predicted by MCM simulations (Figure 4), sequesters RO₂ radicals from the reaction mixture, terminating the oxidation chain and decreasing the extent to which subsequent chemistry occurs over the timescales of the experiments. 4,14,20

343

344

345

346

347

348

326

328

329

330

331

332

333

334

335

336

337

338

339

340

341

342

Implications

These results are broadly consistent with previous studies that demonstrate the importance of NO_x in controlling product distributions, beyond the prevailing RO_2 + NO reaction in "high NO" systems. Hoffmann et al.²¹ explored the effects of NO_x on the relative concentrations of secondary oxidants, and the subsequent influence on SOA formation. A number of recent studies

have examined the specific role that PAN formation and the NO/NO₂ ratio may play in laboratory studies of hydrocarbon oxidation. Chan et al.¹⁹ demonstrated the importance of the NO/NO₂ ratio in governing SOA production from isoprene oxidation, in which PAN is an intermediate in SOA formation. Specifically, they found that even under high NO conditions, low NO/NO₂ ratios foster increased production of PAN, which subsequently contributes to SOA generation. Rissanen et al.²⁰ expanded on that work by characterizing the individual contributions of NO and NO₂ in the formation of highly oxidized multifunctional compounds (HOMs), finding that the NO/NO₂ ratio effectively controls the identities of HOMs in oxidation systems. Similarly, the modeling study of Peng et al.⁴ highlighted the importance of accurately representing NO_x chemistry (including PAN formation) and oxidant levels in oxidation flow reactors (typically used for measurements of SOA formation) in order to reflect atmospheric conditions.

This work builds onto these previous studies by showing that the entire product distribution (not only the formation of HOMs and SOA) can be impacted by NO_x effects that go beyond the standard RO₂ branching (RO₂ + NO vs. RO₂ + HO₂ vs. RO₂ isomerization). We find that, even in a high NO regime, a lower NO/NO₂ ratio fosters higher concentrations of secondary OH, higher PAN concentrations, and a more highly oxidized product distribution. Together, these results can affect the entire product distribution in chamber experiments, leading to a potential disconnect between chamber results and product distributions expected in the atmosphere.

PAN plays an important role in atmospheric systems by sequestering HO_x and NO_x, thereby influencing the kinetics of organic carbon evolution. Here, PAN formation is observed to be highly sensitive to the NO/NO₂ ratio. Under lower-NO conditions, PAN is observed to form preferentially, causing the sequestration of RO₂ radicals and limiting the extent of subsequent chemistry. As such, PAN formation can affect SOA formation, even when it does not serve as a

direct intermediate in SOA formation (as is the case in isoprene oxidation¹⁹). This has implications for recreating high-NO atmospheric conditions in chamber experiments. Specifically, when trying to achieve "polluted conditions" it is not sufficient to flood the reactor with NO; while this ensures that RO₂ + HO₂ and RO₂ isomerization reactions cannot compete with RO₂ + NO, it risks leading to PAN concentrations that may not be representative of atmospheric conditions. Rather, the atmospheric NO/NO₂ ratio has an important influence on the relevance of chamber results to atmospheric conditions; a lower NO/NO₂ ratio results in increased levels of SOA (via the increasingly competitive RO₂ + NO₂ reaction channel), while a higher NO/NO₂ ratio results in fewer products and lower mean oxidation states. This work therefore highlights the need for experimental studies of product distributions and SOA formation to be carried out under atmospherically relevant NO/NO₂ ratios. This has been suggested previously for the accurate simulation of SOA and HOM formation; here we show the use of atmospherically relevant NO/NO₂ ratios is important in virtually all oxidation systems, in order to better simulate the complex, multiphase product distributions generated during atmospheric oxidation processes. It is thus important that laboratory product studies be carried out under conditions in which both the NO/NO₂ ratio and RO₂ chemistry are accurately representative of the atmosphere. Both the absolute NO_x level and the NO/NO₂ ratios may be important in controlling product distributions, and future study of these effects should focus on how product distributions depend on both.

390

391

392

393

394

372

373

374

375

376

377

378

379

380

381

382

383

384

385

386

387

388

389

Supporting Information

Further information regarding the molecular assignments of PTR data; concentrations of NO and NO₂ for each of the experiments (Table S1; Figures S1-2); discussion of wall and tubing losses (Figure S3); deconvolution of precursor and product contributions to C₄H₉O⁺ (Figure S4); PTR

stacked plots for *n*-butyl nitrite photolysis (Figure S5); concentrations, sources, and sinks of OH in *n*-butyl nitrite photolysis as predicted by MCM simulations (Figure S6); experimental uncertainty and reproducibility (Figure S7); C₄H₇O⁺ product time series under different NO/NO₂ ratios (Figure S8); oxidation states of gas-phase product distributions (Figure S9); detailed correlation plots for the photolysis of *n*-butyl nitrite (Figure S10); product distributions from the photolysis *n*-pentyl nitrite (Figures S11-12).

401

402

395

396

397

398

399

400

Acknowledgments.

- This work was supported by NSF grant CHE-1709993. The authors also wish to acknowledge Josh
 Moss for his insight on MCM simulations and PTR fragmentation patterns; Andrew Lambe and
- 405 Anthony Carrasquillo for their assistance in precursor synthesis; and Megan Claflin for sharing
- 406 her knowledge on detection of alkyl nitrites in the PTR.

407

408

References

- 409 (1) Lannuque, V.; Camredon, M.; Couvidat, F.; Hodzic, A.; Valorso, R.; Madronich, S.;
- Bessagnet, B.; Aumont, B. Exploration of the Influence of Environmental Conditions on
- 411 Secondary Organic Aerosol Formation and Organic Species Properties Using Explicit
- Simulations: Development of the VBS-GECKO Parameterization. *Atmos. Chem. Phys.*
- **2018**, *18* (18), 13411–13428.
- 414 (2) Goldstein, A. H.; Galbally, I. E. Known and Unexplored Organic Constituents in the
- 415 Earth's Atmosphere. *Environ. Sci. Technol.* **2007**, *41* (5), 1514–1521.
- 416 (3) Hallquist, M.; Wenger, J. C.; Baltensperger, U.; Rudich, Y.; Simpson, D.; Claeys, M.;
- Dommen, J.; Donahue, N. M.; George, C.; Goldstein, A. H.; et al. The Formation,

- Properties and Impact of Secondary Organic Aerosol: Current and Emerging Issues.
- 419 Atmos. Chem. Phys. **2009**, 9 (June), 5155–5236.
- 420 (4) Peng, Z.; Lee-Taylor, J.; Orlando, J. J.; Tyndall, G. S.; Jimenez, J. L. Organic Peroxy
- Radical Chemistry in Oxidation Flow Reactors and Environmental Chambers and Their
- 422 Atmospheric Relevance. *Atmos. Chem. Phys.* **2019**, *19* (2), 813–834.
- 423 (5) Orlando, J. J.; Tyndall, G. S. Laboratory Studies of Organic Peroxy Radical Chemistry:
- 424 An Overview with Emphasis on Recent Issues of Atmospheric Significance. *Chem. Soc.*
- 425 Rev. **2012**, 41 (19), 6294–6317.
- 426 (6) Crounse, J. D.; Nielsen, L. B.; Jørgensen, S.; Kjaergaard, H. G.; Wennberg, P. O.
- 427 Autoxidation of Organic Compounds in the Atmosphere. J. Phys. Chem. Lett. 2013, 4
- 428 (20), 3513–3520.
- 429 (7) Lelieveld, J.; Butler, T. M.; Crowley, J. N.; Dillon, T. J.; Fischer, H.; Ganzeveld, L.;
- Harder, H.; Lawrence, M. G.; Martinez, M.; Taraborrelli, D.; et al. Atmospheric Oxidation
- 431 Capacity Sustained by a Tropical Forest. *Nature* **2008**, *452* (7188), 737–740.
- 432 (8) Ren, X.; Harder, H.; Martinez, M.; Lesher, R. L.; Oliger, A.; Shirley, T.; Adams, J.;
- Simpas, J. B.; Brune, W. H. HOx Concentrations and OH Reactivity Observations in New
- 434 York City during PMTACS-NY2001. *Atmos. Environ.* **2003**, *37* (26), 3627–3637.
- 435 (9) Martinsson, J.; Eriksson, A. C.; Nielsen, I. E.; Malmborg, V. B.; Ahlberg, E.; Andersen,
- 436 C.; Lindgren, R.; Nyström, R.; Nordin, E. Z.; Brune, W. H.; et al. Impacts of Combustion
- Conditions and Photochemical Processing on the Light Absorption of Biomass
- 438 Combustion Aerosol. *Environ. Sci. Technol.* **2015**, *49* (24), 14663–14671.
- 439 (10) Tkacik, D. S.; Lambe, A. T.; Jathar, S.; Li, X.; Presto, A. A.; Zhao, Y.; Blake, D. R.;
- 440 Meinardi, S.; Jayne, J. T.; Croteau, P. L.; et al. Secondary Organic Aerosol Formation

- from In-Use Motor Vehicle Emissions Using a Potential Aerosol Mass Reactor. *Environ*.
- 442 Sci. Technol. **2014**, 48 (19), 11235–11242.
- 443 (11) Ortega, A. M.; Day, D. A.; Cubison, M. J.; Brune, W. H.; Bon, D.; De Gouw, J. A.;
- Jimenez, J. L. Secondary Organic Aerosol Formation and Primary Organic Aerosol
- Oxidation from Biomass-Burning Smoke in a Flow Reactor during FLAME-3. *Atmos.*
- 446 Chem. Phys. **2013**, 13 (22), 11551–11571.
- 447 (12) Kroll, J. H.; Ng, N. L.; Murphy, S. M.; Flagan, R. C.; Seinfeld, J. H. Secondary Organic
- Aerosol Formation from Isoprene Photooxidation. *Environ. Sci. Technol.* **2006**, 40 (6),
- 449 1869–1877.
- 450 (13) Crounse, J. D.; Paulot, F.; Kjaergaard, H. G.; Wennberg, P. O. Peroxy Radical
- 451 Isomerization in the Oxidation of Isoprene. *Phys. Chem. Chem. Phys.* **2011**, *13* (30),
- 452 13607–13613.
- 453 (14) Peng, Z.; Jimenez, J. L. Modeling of the Chemistry in Oxidation Flow Reactors with High
- 454 Initial NO. Atmos. Chem. Phys. **2017**, 17 (19), 11991–12010.
- 455 (15) Kroll, J. H.; Seinfeld, J. H. Chemistry of Secondary Organic Aerosol: Formation and
- Evolution of Low-Volatility Organics in the Atmosphere. *Atmos. Environ.* **2008**, *42* (16),
- 457 3593–3624.
- 458 (16) Ziemann, P. J.; Atkinson, R. Kinetics, Products, and Mechanisms of Secondary Organic
- 459 Aerosol Formation. Chem. Soc. Rev. 2012, 41 (19), 6582–6605.
- 460 (17) Arey, J.; Aschmann, S. M.; Kwok, E. S. C.; Atkinson, R. Alkyl Nitrate, Hydroxyalkyl
- Nitrate, and Hydroxycarbonyl Formation from the NOx-Air Photooxidations of C5-C8 n-
- 462 Alkanes. J. Phys. Chem. A **2001**, 105 (6), 1020–1027.
- 463 (18) Zhang, X.; Cappa, C. D.; Jathar, S. H.; McVay, R. C.; Ensberg, J. J.; Kleeman, M. J.;

- Seinfeld, J. H. Influence of Vapor Wall Loss in Laboratory Chambers on Yields of
- 465 Secondary Organic Aerosol. *Proc. Natl. Acad. Sci.* **2014**, *111* (16), 5802–5807.
- 466 (19) Chan, A. W. H.; Chan, M. N.; Surratt, J. D.; Chhabra, P. S.; Loza, C. L.; Crounse, J. D.;
- Yee, L. D.; Flagan, R. C. Role of Aldehyde Chemistry and NOx Concentrations in
- Secondary Organic Aerosol Formation. *Atmos. Chem. Phys.* **2010**, *10*, 7169–7188.
- 469 (20) Rissanen, M. P. NO2 Suppression of Autoxidation Inhibition of Gas-Phase Highly
- Oxidized Dimer Product Formation. ACS Earth Sp. Chem. 2018, 2 (11), 1211–1219.
- 471 (21) Hoffmann, T.; Odum, J. A. Y. R.; Bowman, F.; Collins, D.; Klockow, D.; Flagan, R. C.;
- 472 Seinfeld, J. H. Formation of Organic Aerosols from the Oxidation of Biogenic
- 473 Hydrocarbons. J. Atmos. Chem. 1997, 1, 189–222.
- 474 (22) Kessler, S. H.; Nah, T.; Carrasquillo, A. J.; Jayne, J. T.; Worsnop, D. R.; Wilson, K. R.;
- 475 Kroll, J. H. Formation of Secondary Organic Aerosol from the Direct Photolytic
- 476 Generation of Organic Radicals. J. Phys. Chem. Lett. **2011**, 2 (11), 1295–1300.
- 477 (23) Carrasquillo, A. J.; Hunter, J. F.; Daumit, K. E.; Kroll, J. H. Secondary Organic Aerosol
- 478 Formation via the Isolation of Individual Reactive Intermediates: Role of Alkoxy Radical
- 479 Structure. J. Phys. Chem. A **2014**, 118 (38), 8807–8816.
- 480 (24) Carrasquillo, A. J.; Daumit, K. E.; Kroll, J. H. Radical Reactivity in the Condensed Phase:
- Intermolecular versus Intramolecular Reactions of Alkoxy Radicals. J. Phys. Chem. Lett.
- 482 **2015**, *6* (12), 2388–2392.
- 483 (25) Lim, C. Y.; Hagan, D. H.; Coggon, M. M.; Koss, A. R.; Sekimoto, K.; De Gouw, J. A.;
- Warneke, C.; Cappa, C. D.; Kroll, J. H. Secondary Organic Aerosol Formation from the
- Laboratory Oxidation of Biomass Burning Emissions. *Atmos. Chem. Phys.* **2019**, *19* (19),
- 486 12797–12809.

- 487 (26) Heicklen, J. The Decomposition of Alkyl Nitrites and the Reaction of Alkoxy Radicals. In
- 488 *Advances in Photochemistry*; 1988; Vol. 14, pp 177–272.
- 489 (27) Silvern, R. F.; Jacob, D. J.; Travis, K. R.; Sherwen, T.; Evans, M. J.; Cohen, R. C.;
- Laughner, J. L.; Hall, S. R.; Ullmann, K.; Crounse, J. D.; et al. Observed NO/NO2 Ratios
- in the Upper Troposphere Imply Errors in NO-NO2-O3 Cycling Kinetics or an
- 492 Unaccounted NOx Reservoir. *Geophys. Res. Lett.* **2018**, *45* (9), 4466–4474.
- 493 (28) Denisova, T. G.; Denisov, E. T. Kinetic Parameters of Alkyl, Alkoxy, and Peroxy Radical
- 494 Isomerization. *Kinet. Catal.* **2001**, *42* (5), 620–630.
- 495 (29) Praske, E.; Otkjær, R. V.; Crounse, J. D.; Hethcox, J. C.; Stoltz, B. M.; Kjaergaard, H. G.;
- Wennberg, P. O. Atmospheric Autoxidation Is Increasingly Important in Urban and
- 497 Suburban North America. *Proc. Natl. Acad. Sci.* **2018**, *115* (1), 64–69.
- 498 (30) Otkjær, R. V.; Jakobsen, H. H.; Tram, C. M.; Kjaergaard, H. G. Calculated Hydrogen
- Shift Rate Constants in Substituted Alkyl Peroxy Radicals. J. Phys. Chem. A 2018, 122,
- 500 8665–8673.
- 501 (31) Griffin, R. J.; Cocker, D. R.; Flagan, R. C.; Seinfeld, J. H. Organic Aerosol Formation
- from the Oxidation of Biogenic Hydrocarbons. J. Geophys. Res. 1999, 104 (D3), 3555–
- 503 3567.
- 504 (32) DeCarlo, P. F.; Kimmel, J. R.; Trimborn, A.; Northway, M. J.; Jayne, J. T.; Aiken, A. C.;
- Gonin, M.; Fuhrer, K.; Horvath, T.; Docherty, K. S.; et al. Field-Deployable, High-
- Resolution, Time-of-Flight Aerosol Mass Spectrometer. *Anal. Chem.* **2006**, 78 (24), 8281–
- 507 8289.
- 508 (33) Canagaratna, M. R.; Jimenez, J. L.; Kroll, J. H.; Chen, Q.; Kessler, S. H.; Massoli, P.;
- Hildebrandt Ruiz, L.; Fortner, E.; Williams, L. R.; Wilson, K. R.; et al. Elemental Ratio

- Measurements of Organic Compounds Using Aerosol Mass Spectrometry:
- Characterization, Improved Calibration, and Implications. Atmos. Chem. Phys. 2015, 15
- 512 (1), 253–272.
- 513 (34) Kroll, J. H.; Donahue, N. M.; Jimenez, J. L.; Kessler, S. H.; Canagaratna, M. R.; Wilson,
- K. R.; Altieri, K. E.; Mazzoleni, L. R.; Wozniak, A. S.; Bluhm, H.; et al. Carbon
- Oxidation State as a Metric for Describing the Chemistry of Atmospheric Organic
- 516 Aerosol. *Nat. Chem.* **2011**, *3* (2), 133–139.
- 517 (35) Krechmer, J. E.; Lopez-Hilfiker, F. D.; Koss, A. R.; Hutterli, M.; Stoermer, C.; Deming,
- B.; Kimmel, J. R.; Warneke, C.; Holzinger, R.; Jayne, J.; et al. Evaluation of a New
- Reagent-Ion Source and Focusing Ion–Molecule Reactor for Use in Proton-Transfer-
- 520 Reaction Mass Spectrometry. *Anal. Chem.* **2018**, *90*, 12011–12018.
- 521 (36) Isaacman-VanWertz, G.; Massoli, P.; O'Brien, R. E.; Nowak, J. B.; Canagaratna, M. R.;
- Jayne, J. T.; Worsnop, D. R.; Su, L.; Knopf, D. A.; Misztal, P.; et al. Using Advanced
- Mass Spectrometry Techniques to Fully Characterize Atmospheric Organic Carbon:
- 524 Current Capabilities and Remaining Gaps. *Faraday Discuss.* **2017**, *200*, 579–598.
- 525 (37) Aoki, N.; Inomata, S.; Tanimoto, H. Detection of C1-C5 Alkyl Nitrates by Proton
- Transfer Reaction Time-of-Flight Mass Spectrometry. Int. J. Mass Spectrom. 2007, 263
- 527 (1), 12–21.
- 528 (38) Yuan, B.; Koss, A. R.; Warneke, C.; Coggon, M. M.; Sekimoto, K.; De Gouw, J. A.
- Proton-Transfer-Reaction Mass Spectrometry: Applications in Atmospheric Sciences.
- 530 Chem. Rev. **2017**, 117 (21), 13187–13229.
- 531 (39) Lim, Y. Bin; Ziemann, P. J. Effects of Molecular Structure on Aerosol Yields from OH
- Radical-Initiated Reactions of Linear, Branched, and Cyclic Alkanes in the Presence of

- 533 NOx. Environ. Sci. Technol. **2009**, 43, 2328–2334.
- 534 (40) Lim, Y. Bin; Ziemann, P. J. Products and Mechanism of Secondary Organic Aerosol
- Formation from Reactions of N-Alkanes with OH Radicals in the Presence of NOx.
- 536 Environ. Sci. Technol. **2005**, 39 (23), 9229–9236.
- 537 (41) Hunter, J. F.; Carrasquillo, A. J.; Daumit, K. E.; Kroll, J. H. Secondary Organic Aerosol
- Formation from Acyclic, Monocyclic, and Polycyclic Alkanes. *Environ. Sci. Technol.*
- **2014**, 48 (17), 10227–10234.
- 540 (42) Noyes, W. A. Explanation of the Formation of Alkyl Nitrites in Dilute Solutions; Butyl
- and Amyl Nitrites. J. Am. Chem. Soc. **1933**, 55 (9), 3888–3889.
- 542 (43) Bloss, C.; Wagner, V.; Jenkin, M. E.; Volkamer, R.; Bloss, W. J.; Lee, J. D.; Heard, D. E.;
- Wirtz, K.; Rea, G.; Wenger, J. C.; et al. Development of a Detailed Chemical Mechanism
- 544 (MCMv3.1) for the Atmospheric Oxidation of Aromatic Hydrocarbons. *Atmos. Chem.*
- 545 *Phys.* **2005**, *3* (2002), 641–664.
- 546 (44) Saunders, S. M.; Jenkin, M. E.; Derwent, R. G.; Pilling, M. J. Protocol for the
- Development of the Master Chemical Mechanism, MCM v3 (Part A): Tropospheric
- Degradation of Non-Aromatic Volatile Organic Compounds. *Atmos. Chem. Phys.* **2003**, *3*,
- 549 161–180.
- 550 (45) Wolfe, G. M.; Marvin, M. R.; Roberts, S. J.; Travis, K. R.; Liao, J. The Framework for 0-
- D Atmospheric Modeling (F0AM) v3.1. *Geosci. Model Dev.* **2016**, 9 (9), 3309–3319.
- 552 (46) Calvert, J. G.; Orlando, J. J.; Stockwell, W. R.; Wallington, T. J. *The Mechanisms of*
- *Reactions Influencing Atmospheric Ozone*; Oxford University Press, 2015.
- 554 (47) Demarcke, M.; Amelynck, C.; Schoon, N.; Dhooghe, F.; Rimetz-Planchon, J.; Van
- Langenhove, H.; Dewulf, J. Laboratory Studies in Support of the Detection of Biogenic

556 Unsaturated Alcohols by Proton Transfer Reaction-Mass Spectrometry. Int. J. Mass 557 Spectrom. **2010**, 290 (1), 14–21. Hastie, D. R.; Gray, J.; Langford, V. S.; Maclagan, R. G. A. R.; Milligan, D. B.; Mcewan, 558 M. J. Real-Time Measurement of Peroxyacetyl Nitrate Using Selected Ion Flow Tube 559 560 Mass Spectrometry. Rapid Commun. Mass Spectrom. 2010, 24, 343–348. 561 (49)Hansel, A.; Wisthaler, A. A Method for Real-Time Detection of PAN, PPN and MPAN in 562 Ambient Air. Geophys. Res. Lett. 2000, 27 (6), 895–898. 563 (50)Blake, R. S.; Monks, P. S.; Ellis, A. M. Proton-Transfer Reaction Mass Spectrometry. Chem. Rev. 2009, 109 (0), 861–896. 564

565